

Temperature-dependent transport properties of InAs films grown on lattice-mismatched GaP

V. Gopal

School of Materials Engineering, Purdue University, W. Lafayette, Indiana 47907

V. Souw

Department of Physics, Purdue University, W. Lafayette, Indiana 47907

E.-H. Chen

Department of Electrical Engineering, Yale University, New Haven, Connecticut 06520

E. P. Kvam and M. McElfresh^{a)}

School of Materials Engineering, Purdue University, W. Lafayette, Indiana 47907

J. M. Woodall

Department of Electrical Engineering, Yale University, New Haven, Connecticut 06520

(Received 30 September 1999; accepted for publication 21 October 1999)

Hall effect and electrical resistivity measurements were carried out on undoped InAs thin films grown by molecular-beam epitaxy directly on (001) GaP substrates. The large lattice mismatch between these two compounds results in a high density array of misfit dislocations at the heterointerface and threading dislocations in the InAs epilayer. The threading dislocation density varies with epilayer thickness, with the largest proportion being present near the heterointerface. This leads to variation of both the carrier concentration and electron mobility with thickness. Consequently, a multilayer analysis was used to interpret the transport data. This analysis yields a temperature-independent carrier concentration, which indicates degenerate donor levels in this narrow band-gap material. Room temperature mobilities in excess of $10\,000\text{ cm}^2/\text{V s}$ were obtained for thick InAs layers despite dislocation densities of 10^{10} cm^{-2} . The relative insensitivity of the mobility to temperature suggests that temperature-independent scattering dominates over ionized impurity/defect and phonon scattering. © 2000 American Institute of Physics.

[S0021-8979(00)05603-6]

I. INTRODUCTION

A narrow band gap (0.36 eV) and high bulk electron mobility ($33\,000\text{ cm}^2/\text{V s}$ at 300 K) make InAs a very attractive material for far-infrared detectors as well as for high speed devices. However, InAs device technology has been hampered by the absence of a suitable lattice matched substrate. Considerable effort has been devoted to grow InAs on GaAs substrates by molecular-beam epitaxy (MBE) and other techniques.^{1–3} Misfit and threading dislocations, which arise in the InAs layer as a consequence of the lattice mismatch, have been reported to have a deleterious impact on the electronic properties.^{4,5} Specifically, dislocations act as nonradiative recombination centers in InAs and other direct gap semiconductors, severely degrading light emission efficiency and rendering these materials unsuitable for optoelectronic devices. However, dislocations have not been reported to reduce electron mobility in InAs severely enough to make it unsuitable for high speed and high frequency applications.^{6,7} Consequently, it becomes important to study electron transport in highly dislocated InAs layers.

Previously, transport studies have been performed on InAs grown mainly on GaAs both by MBE^{6–11} and by metal organic chemical vapor deposition (MOCVD).^{12–14} To a lim-

ited extent, InAs/Si heterostructures have also been studied.¹⁵ However, detailed microstructure characterization and a correlation with electrical properties has not been attempted. We have recently demonstrated the MBE growth of InAs on GaP.¹⁶ This system has a lattice mismatch of 11.2%, which results in very high misfit and threading dislocation densities. The growth of InAs on GaP is initially in the form of islands, but unlike many other highly mismatched systems, island coalescence occurs at a very early stage—by a nominal thickness of 5 nm. Thus, it is possible to fabricate and characterize both very thin layer samples, with a high defect content, as well as thicker layer samples with fewer defects.

A combination of Hall effect and electrical resistivity measurements can be used to obtain carrier type, concentration, and mobility. However, the interpretation of such data is complicated by microstructural nonuniformity. The Fermi level of the free surface in InAs is known to be pinned in the conduction band, resulting in surface carrier accumulation.¹³ To account for this, transport in InAs has been analyzed by two-layer models, one a uniform bulk layer and the other a surface layer. The samples used in the present work were designed to avoid surface pinning and conduction by means of a wider gap $\text{Al}_{0.2}\text{In}_{0.8}\text{As}$ capping layer. Hence, the properties of the InAs epilayer alone can be studied, without the complications of a surface layer. Due to the nonuniformity of the dislocation microstructure, the assumption of a uniform

^{a)}Also at Department of Physics, Purdue University, W. Lafayette, IN 47907.

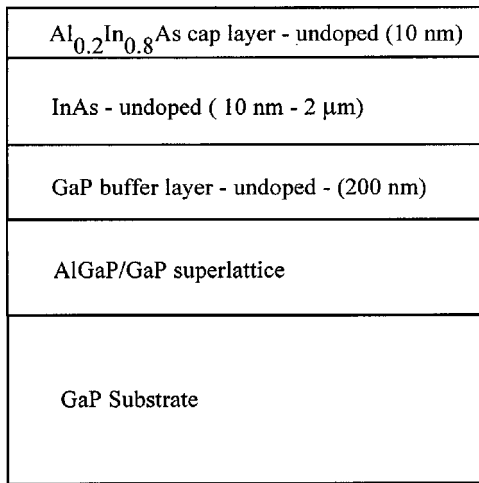


FIG. 1. Schematic of multilayer structure grown by MBE.

bulk layer cannot be made. A multilayer analysis has been used here to model transport properties of InAs.

II. EXPERIMENT

InAs layers were grown on commercially obtained (001) GaP substrates by solid-source MBE using a Varian GEN-II system. The substrates were thermally cleaned at 710 °C under P₂ overpressure. A 20 period superlattice consisting of 5 nm alternating layers of GaP and AlP was grown to prevent the outdiffusion of impurities from the substrate. This was followed by the growth of a 200 nm buffer layer of undoped GaP at 660 °C. The substrate temperature was lowered to 350 °C for the growth of InAs. The initial few monolayers were grown under In rich conditions as this was found to promote a smoother surface. Reflection high-energy electron diffraction was used to monitor surface morphology and growth rate *in situ*. Atomic force microscopy and cross-sectional transmission electron microscopy (TEM) were used *ex situ* to confirm morphology and thickness. Finally, an undoped, 5 nm capping layer of Al_{0.2}In_{0.8}As was deposited. Six samples of varying InAs layer thickness, 10, 20, 250, 500, 1000, and 2000 nm, were used in this study. Figure 1 is a schematic diagram of the multilayer structure.

Microstructural characterization was performed using a JEOL 2000 FX TEM with an accelerating voltage of 200 kV. Both cross-section and plan-view imaging were used to study the distribution of dislocations in the epilayer. Figure 2 is a cross-section micrograph of a 2 μm InAs layer grown on GaP. The nonuniformity of the dislocation microstructure is apparent. The defect density is very high in the near-interface region and decreases away from the interface. The greatest variation in dislocation density occurs in the initial 0.25 μm, beyond which a more uniform density persists. Figure 3 is a plan-view micrograph of the 1 μm sample, from which the near-surface threading defect density is estimated to be $\sim 10^{10} \text{ cm}^{-2}$.

Hall voltage and resistivity measurements were performed using the van der Pauw technique. Approximately square specimens were cleaved, and indium contacts were pressed at the four corners. Hall voltage and resistivity mea-

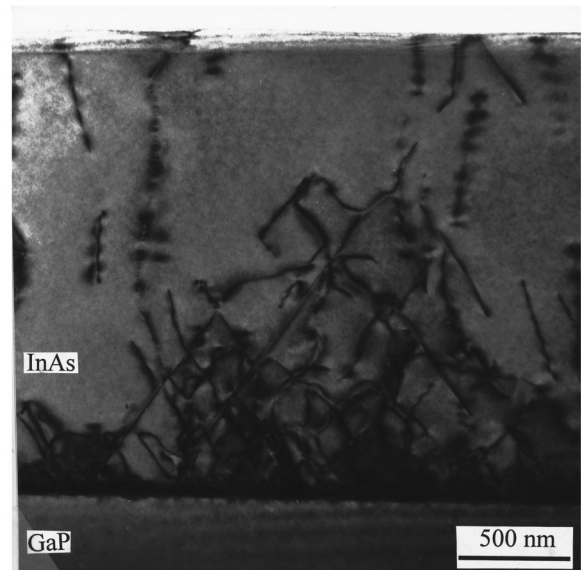


FIG. 2. Cross-section TEM micrograph of a 2 μm InAs/GaP heterostructure.

surements were then performed over the temperature range from 3 to 300 K in both zero magnetic field and 0.5 T, where the Hall voltage is still linear with magnetic field. The temperature and magnetic field were controlled by a Quantum Design PPMS system with a superconducting magnet. A fixed transport current of 25 μA was used, well within the ohmic regime of the samples' *I*-*V* curve. The sign of the

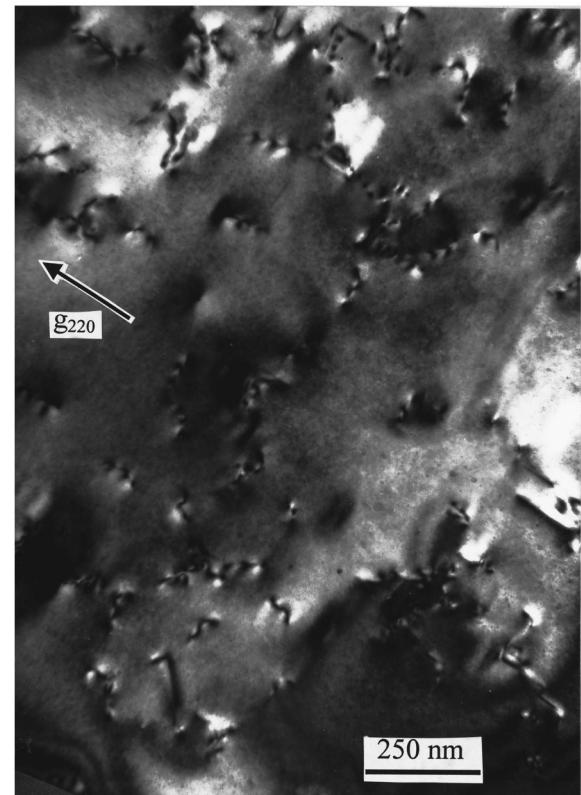


FIG. 3. 220 dark-field plan-view micrograph of a 1 μm InAs layer. The threading dislocation density is estimated to be $\sim 10^{10} \text{ cm}^{-2}$.

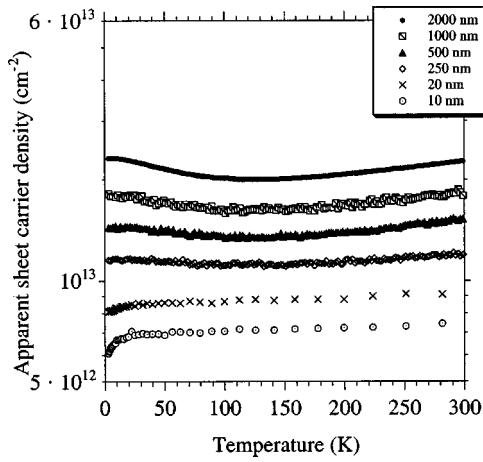


FIG. 4. Variation of the apparent (as measured) sheet carrier density with temperature for each sample.

Hall coefficient indicated that the majority carriers were electrons for each of the samples.

III. RESULTS

Figure 4 plots the apparent sheet carrier density, N_s^a , against temperature for each sample. N_s^a is obtained directly from the measured Hall coefficient, R_s , via $N_s^a = 1/(eR_s)$. N_s^a is very high even for the thinnest sample ($\sim 7 \times 10^{12} \text{ cm}^{-2}$, for the 10 nm sample), and as the sample thickness increases, N_s^a increases quickly for thin samples, but relatively slowly for thicker samples. This suggests a very high interfacial contribution and a drop to a lower background bulk value as sample thickness increases.

The temperature dependence of N_s^a is qualitatively similar to previously published data.^{6–15} We believe that this temperature dependence does not indicate thermal activation, but instead reflects the fact that N_s^a is a function of the carrier density weighted by the mobility.

Figure 5 shows the apparent mobility, μ^a , as a function of temperature for samples of different thickness. μ^a is cal-

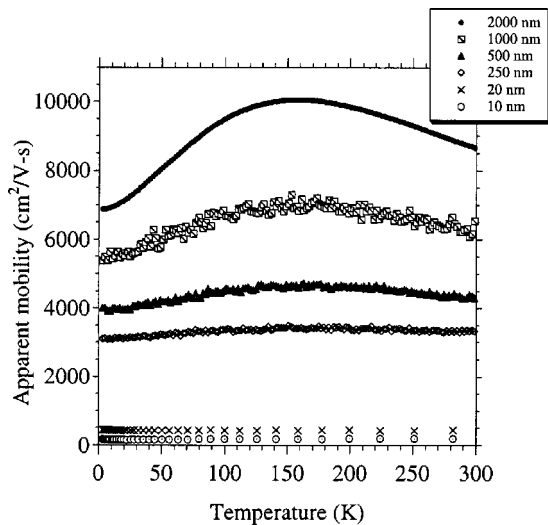


FIG. 5. Variation of the apparent (as measured) mobility with temperature for each sample.

culated directly from the measured Hall coefficient (R_s) and the zero-field conductivity, σ_s , via $\mu^a = R_s \sigma_s$. The apparent mobility clearly increases with sample thickness and shows only a small temperature dependence for samples thinner than 250 nm. For samples thicker than 250 nm, a very broad maximum occurs near $T = 175 \text{ K}$.

IV. INTERPRETATION OF HALL EFFECT DATA

In a nonuniform layer where the mobility (μ) and carrier concentration (n) vary with thickness, the standard interpretation of Hall effect data provides only an apparent or weighted average value of these quantities. In this case, the measured Hall coefficient (R_s) and sheet conductivity (σ_s) are given by^{17,18}

$$R_s = \frac{\int n(x)\mu(x)^2 dx}{e[\int n(x)\mu(x) dx]^2}, \quad (1)$$

$$\sigma_s = e \int n(x)\mu(x) dx, \quad (2)$$

where e is the electronic charge and x is the distance perpendicular to the interface. Then, the apparent sheet carrier density and mobility are

$$N_s^a = \frac{1}{eR_s} = \frac{[\int n(x)\mu(x) dx]^2}{\int n(x)\mu(x)^2 dx}, \quad (3)$$

$$\mu^a = R_s \sigma_s = \frac{\int n(x)\mu(x)^2 dx}{\int n(x)\mu(x) dx}. \quad (4)$$

However, the true sheet carrier density and the average mobility can differ considerably from the apparent (measured) values:

$$N_s = \int n(x) dx, \quad (5)$$

$$\mu_{av} = \frac{\int n(x)\mu(x) dx}{\int n(x) dx}. \quad (6)$$

Hence, large variations in mobility could cause N_s^a to be dominated by a small fraction of carriers which have a high mobility. This was pointed out by Watkins *et al.*,^{13,14} but in the context of a competition between bulk and surface conduction.

The apparent values defined above can be used to extract the Hall mobility and carrier density distributions. Differentiating Eqs. (1) and (2) and rearranging terms yields

$$\mu_H(x) = \frac{d(R_s \sigma_s^2)/dx}{d\sigma_s/dx}, \quad (7)$$

$$n(x) = \frac{[d\sigma_s/dx]^2}{e[d(R_s \sigma_s^2)/dx]}. \quad (8)$$

To account for a finite data set, the derivatives are approximated by differentials, as

$$d\sigma_s/dx \approx \Delta(\sigma_s)_i/\Delta x_i \quad (9)$$

and

$$d(R_s \sigma_s^2)/dx \approx \Delta(R_s \sigma_s^2)_i/\Delta x_i.$$

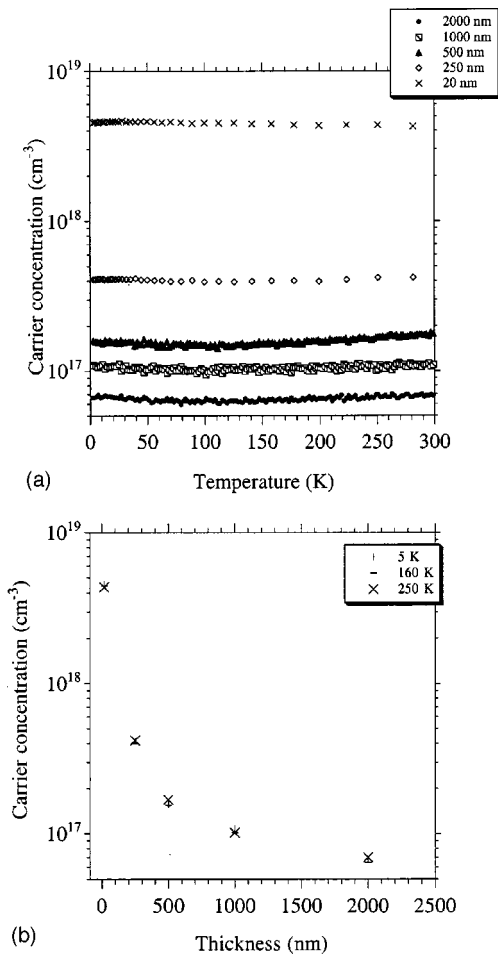


FIG. 6. (a) Variation of the extracted carrier density with temperature and epilayer thickness. (b) Variation of the extracted carrier density with thickness at three different temperatures. The carrier density reaches a limiting value of $\sim 6 \times 10^{16} \text{ cm}^{-3}$.

Ideally, a thin layer of material is etched and the measurements are repeated after each etch step to obtain the distributions. Unfortunately, in the present case, an etch would first remove the Al_{0.2}In_{0.8}As capping layer and introduce surface carrier accumulation in the InAs. Hence, measurements were performed separately on a number of as-grown samples of varying InAs layer thickness.

V. DISCUSSION

A. Variation of carrier concentration with thickness and temperature

Figure 6(a) plots the extracted carrier concentration, $n(x)$, versus temperature for each sample thickness. $n(x)$ is calculated from N_s^a in Fig. 4 using Eqs. (8) and (9). Very little temperature dependence is exhibited by $n(x)$, suggesting that the defect level(s) responsible for carrier generation are degenerate. This is not surprising since InAs is a very narrow band-gap semiconductor.

Figure 6(b) plots n as a function of sample thickness at $T=5, 160,$ and 250 K . There is a steep drop in carrier concentration away from the interface and, at a thickness of $2 \mu\text{m}$, n appears to reach limiting value of $\sim 6 \times 10^{16} \text{ cm}^{-3}$ at all three temperatures. The thickness variation of $n(x)$ cor-

relates well with the observed dislocation microstructure. A very high dislocation density exists near the interface, which drops and also reaches a limiting value ($\sim 10^{10}$ dislocations/cm²) far from the interface, as seen in Fig. 3. Thus, it is likely that carrier generation is defect related.

We have previously proposed that the high interfacial sheet carrier density could be caused by a structural donor source at the intersection of misfit dislocations at the InAs/GaP interface and have demonstrated a one-to-one correspondence between the density of the intersection sites and the observed N_s .¹⁹ Although the carriers in the bulk could also be related to dislocations, a one-to-one correspondence does not exist in this case. A simple calculation, based on an estimated constant dislocation density of 10^{10} cm^{-2} and assuming complete ionization of all atoms along each dislocation line, yields a carrier density of $\sim 5 \times 10^{17} \text{ cm}^{-3}$, an order of magnitude higher than the extracted background concentration of $6 \times 10^{16} \text{ cm}^{-3}$. This difference is unlikely to be caused by compensating point defects. Compensating charge centers would result in very low effective mobility, contrary to our observation of monotonically increasing mobility with thickness, to values in excess of $14000 \text{ cm}^2/\text{V s}$.

It is more likely that the dislocation cores in InAs do not have charged centers associated with them along their entire length. For instance, carrier generation could be restricted to kink sites associated with threading dislocations. Alternately, charged native defects could be responsible, in which case the correspondence between dislocation density and carrier density suggests that the distribution of native defects is influenced by dislocations.

B. Variation of mobility with thickness and temperature

In Fig. 7(a), the extracted mobility, $\mu(x)$, is plotted versus temperature for each sample thickness. $\mu(x)$ is calculated from the apparent mobility (see Fig. 5) and Eq. (7). At very small thickness, mobility is essentially independent of temperature; even at $2 \mu\text{m}$, the temperature dependence is not very strong. There is a very broad peak in the mobility at about 175 K for the thicker samples. Figure 7(b) plots μ as a function of sample thickness at $T=5, 160,$ and 250 K . The mobility increases with thickness and appears to saturate to a value in excess of $10000 \text{ cm}^2/\text{V s}$ at $2 \mu\text{m}$.

The variation of mobility with temperature in semiconductors yields information on competing scattering mechanisms. The present system is unusual due to the rather low temperature sensitivity of the mobility.

It is commonly accepted that the two most important mechanisms in semiconductors that limit mobility are ionized impurity scattering and phonon scattering.²⁰ Complete expressions for μ_{imp} and μ_{pho} are available,²¹⁻²³ but it can be shown that the temperature dependence for these mechanisms are

$$\begin{aligned} \mu_{\text{imp}} &\propto T^{3/2} \quad \text{for ionized impurity scattering,} \\ \mu_{\text{pho}} &\propto T^{-3/2} \quad \text{for phonon scattering.} \end{aligned} \tag{10}$$

Kalem *et al.*⁶ reported that the former is dominant for $T < 100 \text{ K}$ and the latter for $T > 100 \text{ K}$.

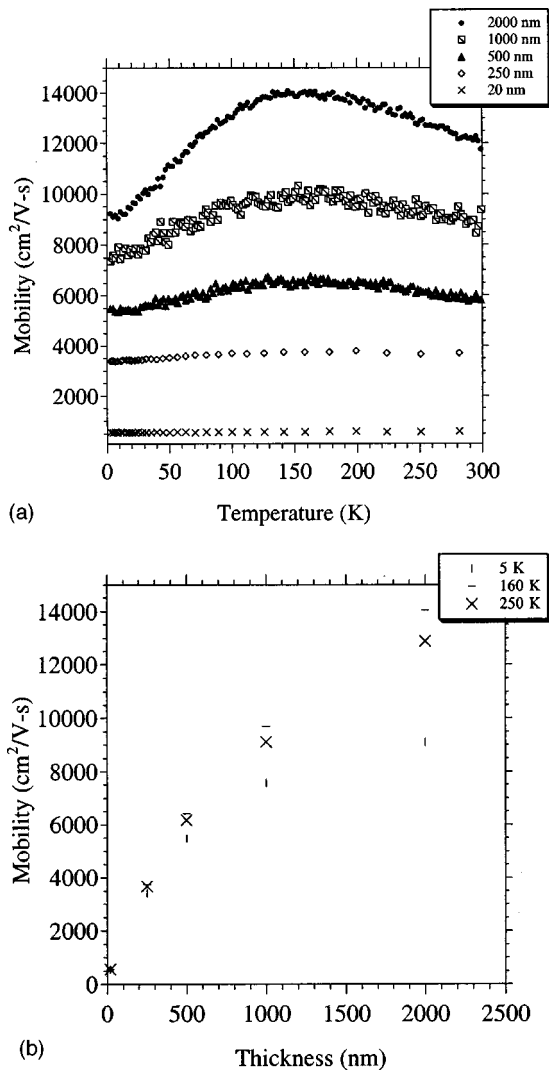


FIG. 7. (a) Variation of the extracted carrier mobility with temperature and epilayer thickness. (b) Variation of the extracted mobility with thickness at three different temperatures. The mobility reaches a limiting value in excess of 10 000 cm²/V s.

The exceptionally weak temperature dependence in Fig. 7(a) leads to power-law exponents much smaller in magnitude than 1.5. The 2 μm sample, which displayed the greatest temperature sensitivity, had a low temperature exponent of ~ 0.2 and a high temperature exponent of ~ -0.3 . These exponents are also much lower than previously reported by Kalem *et al.*, who deduced ~ 0.6 for ionized impurity scattering and ~ -1.1 for phonon scattering.⁶ To account for the deviation from 1.5, it was proposed that dislocation lines were charged, and that the potential due to the space charge region around them scattered electrons with a smaller temperature dependence.⁶⁻⁸ Watkins *et al.* also reported much stronger temperature dependence than observed here.^{13,14}

We propose here that a temperature-independent scattering mechanism is superposed on the ionized impurity and phonon scattering mechanisms. The resulting total mobility is then

$$\mu_{\text{total}}^{-1} = \mu_{\text{imp}}^{-1} + \mu_{\text{pho}}^{-1} + \mu_{\text{TI}}^{-1}. \quad (11)$$

The relative temperature insensitivity of μ points to the dominance of the third, temperature-independent, scattering mechanism over ionized impurity and phonon scattering in this system.

Possible contributing mechanisms to this strong temperature independent scattering are structural features, inhomogeneously arrayed, that limit the carrier mean free path. These may include:

(i) Surface roughness: The 10 and 20 nm thick samples have very similar defect contents. It has been observed that InAs grows in Volmer-Weber (island) mode on GaP.²⁴ Island coalescence occurred by a nominal thickness of 5 nm, but surface roughness persists. Atomic force microscopy (AFM) measurements indicate that the 10 nm sample has a rougher surface morphology (and a rougher AlInAs/InAs interface) than the 20 nm sample. This would account for the lower mobility of the former. Surface roughness related scattering is not expected to have explicit temperature dependence. As used in this context, surface roughness does not refer to the cross-hatch problem seen in lower lattice mismatch systems.²⁵ Since strain relaxation at the InAs/GaP interface is mainly by a sessile network of 90° misfit dislocations, crosshatch is eliminated. Due to the larger volume available for conduction, roughness related scattering in this system is not a major contributor for the thick samples.

(ii) Dislocation strain fields: Threading and misfit dislocations have associated strain fields around them, which can interact with and scatter electrons. Since mobility is lower and less sensitive to temperature in the highly dislocated thinner samples as compared to the thicker samples, it can be surmised that strain field related scattering is significant. Kalem *et al.* who observed much stronger temperature dependence, also observed much lower dislocation densities ($\sim 10^7 \text{ cm}^{-2}$) in their thick InAs/GaAs samples, and hence this effect may have manifested itself, but not as strongly.⁶⁻⁸

(iii) Neutral impurities: Neutral impurities are believed to cause temperature-independent scattering.²¹ These could include neutral vacancies and iso-electronic substitutional elements, for instance, Al or Ga on an In site.

Preliminary Hall effect measurements on 1 and 2 μm thick InAs layers grown at a higher substrate growth temperature (480 °C) resulted in lower carrier concentration, higher peak mobility ($>20\,000 \text{ cm}^2/\text{V s}$), and more pronounced temperature dependence of mobility than displayed by the 350 °C grown samples. TEM images show a reduction in threading dislocation density. A more detailed investigation of samples grown at different temperatures is underway and will help clarify the issue of temperature-independent scattering in InAs.

VI. CONCLUSION

The transport properties of undoped InAs epilayers grown on lattice-mismatched GaP substrates were investigated by variable temperature Hall effect and resistivity measurements. Multilayer analysis of the Hall data showed that carrier concentration does not have a significant dependence on temperature, regardless of the thickness. A linkage was drawn between carrier generation and dislocation density in

InAs. The variation of mobility with temperature indicated the dominance of temperature-independent scattering mechanisms over ionized impurity and phonon scattering contributions. Different mechanisms for temperature-independent scattering were discussed, including surface and interface roughness scattering, dislocation strain field scattering, and neutral impurity scattering.

ACKNOWLEDGMENT

This work was partially supported by the NSF through Grant No. DMR 9400415.

- ¹C. Chang, C. M. Serrano, L. L. Chang, and L. Esaki, *Appl. Phys. Lett.* **37**, 538 (1980).
- ²J. M. Gerard and J. Y. Marzin, *Appl. Phys. Lett.* **53**, 568 (1988).
- ³H. Wang, T. Fan, J. Wu, Y. Zeng, J. Dong, and M. Kong, *J. Cryst. Growth* **186**, 38 (1998).
- ⁴D. L. Dexter and F. Seitz, *Phys. Rev.* **86**, 964 (1952).
- ⁵R. J. Egan, V. W. L. Chin, and T. L. Tansley, *J. Appl. Phys.* **75**, 2473 (1994).
- ⁶S. Kalem, J.-I. Chyi, H. Morkoc, R. Bean, and K. Zanio, *Appl. Phys. Lett.* **53**, 1647 (1988).
- ⁷S. Kalem, *J. Appl. Phys.* **66**, 3097 (1988).
- ⁸S. Kalem, *Semicond. Sci. Technol.* **5**, S200 (1990).
- ⁹S. Holmes, R. A. Stradling, P. D. Wang, R. Droopad, S. D. Parker, and R. L. Williams, *Semicond. Sci. Technol.* **4**, 303 (1989).
- ¹⁰P. D. Wang, S. N. Holmes, T. Le, R. A. Stradling, I. T. Ferguson, and A. G. de Oliveira, *Semicond. Sci. Technol.* **7**, 767 (1992).
- ¹¹Z. Hongwei, Z. Yiping, W. Hongmei, D. Jianrong, Z. Zhanping, P. Liang, and K. Meiyang, *J. Cryst. Growth* **191**, 361 (1998).
- ¹²J. R. Sites and H. H. Wieder, *CRC Crit. Rev. Solid State Mater. Sci.* **5**, 385 (1975).
- ¹³S. P. Watkins, C. A. Tran, R. Ares, and G. Soerensen, *Appl. Phys. Lett.* **66**, 882 (1995).
- ¹⁴S. P. Watkins, C. A. Tran, G. Soerensen, H. D. Cheung, R. A. Ares, Y. Lacroix, and M. L. W. Thewalt, *J. Electron. Mater.* **24**, 1583 (1995).
- ¹⁵S. Kalem, J. Chyi, C. W. Litton, H. Morkoc, S. C. Kan, and A. Yariv, *Appl. Phys. Lett.* **53**, 562 (1988).
- ¹⁶V. Gopal, E. P. Kvam, T. P. Chin, and J. M. Woodall, *Appl. Phys. Lett.* **72**, 2319 (1998).
- ¹⁷R. L. Petritz, *Phys. Rev.* **110**, 1254 (1958).
- ¹⁸R. Baron, G. A. Shifrin, O. J. Marsh, and J. W. Mayer, *J. Appl. Phys.* **40**, 3702 (1969).
- ¹⁹V. Gopal, E.-H. Chen, E. P. Kvam, and J. M. Woodall, *J. Vac. Sci. Technol. B* **17**, 1767 (1999).
- ²⁰L. Solymar and D. Walsh, *Lectures on the Electrical Properties of Materials* (Oxford University Press, London, 1993), pp. 163–165.
- ²¹J. M. Ziman, *Electrons and Phonons* (Oxford University Press, London, 1962), pp. 428–438.
- ²²H. Brooks, *Advances in Electronics and Electron Physics* (Academic, New York, 1955), Vol. 5, p. 85.
- ²³P. C. Mathur, R. Shyam, and S. Jain, *Phys. Status Solidi A* **50**, 11 (1978).
- ²⁴E.-H. Chen, Ph.D. thesis, Purdue University, 1998.
- ²⁵J. W. P. Hus, E. A. Fitzgerald, Y. H. Xie, P. J. Silverman, and M. J. Cardillo, *Appl. Phys. Lett.* **61**, 1293 (1992).